06

Formation of $(Co_{40}Fe_{40}B_{20})_x(LiNbO_3)_{100-x}$ composite film on a metallic substrate

© A.V. Sitnikov,[1,2] I.V. Babkina,[1] Yu.E. Kalinin,[1] A.E. Nikonov,[1] M.N. Kopytin,[1] A.R. Shakurov,[1] O.I. Remizova,[1] L.I. Yanchenko[1]

[1] Voronezh State Technical University,
394026 Voronezh, Russia
[2] National Research Center „Kurchatov Institute“,
123182 Moscow, Russia
e-mail: michaelkopitin@mail.ru

Received April 11, 2022
Revised May 11, 2022
Accepted May 12, 2022

The topological features of the formation of $(Co_{40}Fe_{40}B_{20})_{15}(LiNbO_3)_{85}$ composite films deposited by ion-beam method on a metal electrode Cr/Cu/Cr has been investigated. The presence of a dielectric layer between the upper Cr layer and the CoFe−$LiNbO_3$ film with a thickness of $d_{ox} \approx 15$ nm has been established. The difference in the size of granules near the amorphous layer and in the volume of the film has been shown. A model of the formation of $(Co_{40}Fe_{40}B_{20})_x(LiNbO_3)_{100-x}$ nanocomposite film at the initial stage of growth has been proposed. It has been shown that the formation of α-$LiNbO_3$ layer on the chrome metal film surface is possible with the realization of island and layer-by-layer growth mechanisms for various phases of the composite.

Keywords: nanocomposite, growth mechanisms, self-organization, structure.

DOI: 10.21883/TP.2022.09.54683.94-22

Introduction

In recent years intensive studies has been carried out on nanocomposites from metal granules in an oxide matrix during the development of memristive elements in terms of their use as a functional medium [1–3]. Good memristive properties were found in nanogranular composites $(Co_{40}Fe_{40}B_{20})_x(LiNbO_3)_{100-x}$: ratio of electrical resistances in high-resistance and low-resistance states $R_{off}/R_{on} > 100$, maximum switching cycles number $N_{max} > 10^5$ [4–6]. The effect of reversible resistive switching (RS) from one state (high-resistance) to another (low-resistance) and back under the action of a switching potential with changing polarity implies the anisotropic properties of the functional medium or the material of electrical contacts. In the first case, the main switching mechanism is the formation of conducting channels from oxygen vacancies in high-resistivity oxide, when two layers with different oxidation states are formed in the composite film [7–11]. In the case when the effect is associated with the electrical migration of metal atoms into a dielectric film, the difference in the material of the electrodes of the upper and lower contacts is critical [12–15].

In the case of nanocomposites $(Co_{40}Fe_{40}B_{20})_x(LiNbO_3)_{100-x}$ the material of the electrodes does not have a decisive effect on the presence of memristive properties, and resistive switching is determined by the high-resistance layer of the composite. In this case, the degree of oxidation and the gradient of the degree of oxidation of the composite through the film thickness have a more significant influence on the parameters of the observed effect. However, the structural features and reasons for the formation of the heterogeneous structure of composites $(Co_{40}Fe_{40}B_{20})_x(LiNbO_3)_{100-x}$, which determine the presence of the memristive effect in these heterogeneous systems, are not identified completely.

Taking into account the above, the purpose of this work is to reveal the type and physical reasons for the heterogeneity of the structure of nanocomposite films $(Co_{40}Fe_{40}B_{20})_x(LiNbO_3)_{100-x}$ obtained by ion-beam sputtering during their growth on a metal surface as a result of the self-organization process.

1. Experimental procedure

Films of nanocomposites $(Co_{40}Fe_{40}B_{20})_x(LiNbO_3)_{100-x}$ were obtained by the method of ion-beam sputtering [16,17]. The target consisted of a metal base of the $Co_{40}Fe_{40}B_{20}$ alloy with a size of $270 \times 80 \times 15$ mm, on the surface of which 15 plates of monocrystal compound $LiNbO_3$ with the size $80 \times 10 \times 2$ mm were fixed unevenly along the length of the target. Sitall (glass-ceramic) plates with a metal film preliminarily deposited on their surface were chosen as the substrate. The Cr/Cu/Cr system was chosen as the metal sublayer (electrode). This film was deposited on the substrate by sequential sputtering of the corresponding targets in one technological cycle. Four glass-ceramic substrates were arranged in a row along the target axis, creating an application area of 240×48 mm. This arrangement of the mosaic target and substrates made it possible, in one technological cycle, to obtain samples with different ratio of the dielectric and metallic phase

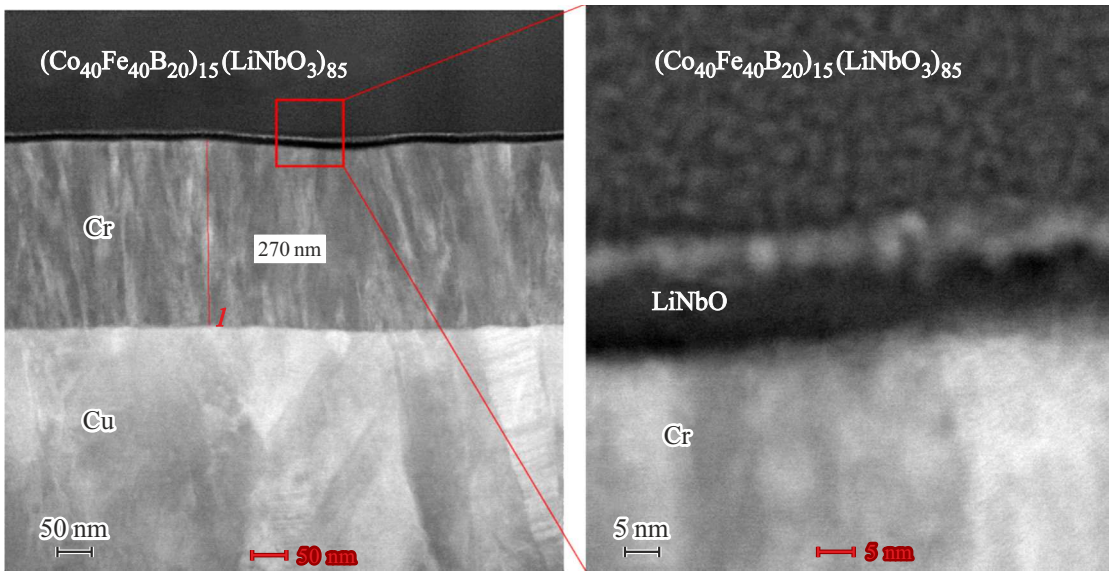

Figure 1. STEM-cross-sectional image of $(Co_{40}Fe_{40}B_{20})_{15}(LiNbO_3)_{85}$/Cr/Cu composite structure.

depending on the relative position of the target–substrate. The thickness of the composite film was $\sim 1.5\,\mu$m.

High-resolution images obtained by transmission electron microscopy (TEM) and scanning transmission electron microscopy (STEM), electron diffraction patterns from the selected area and microanalysis were recorded using a transmission/scanning electron microscope (T/SEM) Tecnai Osiris (Thermo Fisher Scientific, USA) at an accelerating voltage of 200 keV, equipped with an energy-dispersive X-ray spectrometer (EDS) Super-X (Bruker, USA) and a large-angle ring dark-field detector (LRDD) (Fischione, USA).

2. Experimental results

The electrical properties of metal–dielectric nanocomposites in the case of electrical transfer perpendicular to the plane of the film are mainly determined by the heterogeneity of the formation of the heterogeneous system structure during synthesis; therefore, the TEM method was used to study the cross section of the metal–nanocomposite–metal(M/NC/M) structure (Fig. 1), which revealed a number of interesting features of the evolution of NC $(Co_{40}Fe_{40}B_{20})_{15}(LiNbO_3)_{85}$ growth. Thus, an amorphous layer with a thickness of $d_{ox} \approx 15$ nm was found at the interface between Cr and the NC film.

A more detailed analysis of the structural and phase features of this object was presented in the paper [4]. The analysis of the elements distribution in the geometry transverse to the interlayer by scanning electron microscopy (SEM) showed that in the region of the amorphous layer the concentration of Nb is 25 at.% and of O — 75 at.%. In this case, the content of Fe and Co is significantly lower than in the bulk of the nanocomposite layer. Therefore, we can conclude that the detected interlayer is an amorphous compound $LiNbO_3$. A relatively sharp interface is observed between the lower electrode layer of Cr and $LiNbO_3$, indicating the absence of interdiffusion.

In the same paper it was revealed that the average size of CoFe granules directly adjacent to the dielectric layer is ~ 6 nm, and this is much larger than the metal particles in the film bulk, whose size is ~ 3 nm. The high-resolution TEM image showed that $LiNbO_3$ matrix is amorphous, while the CoFe nanogranules are crystalline. Electrons microdiffraction showed that CoFe nanogranules have a BCC crystal structure with a lattice parameter $a_c = 0.29$ nm.

Thus, the performed structural studies showed that at the initial stage of $(Co_{40}Fe_{40}B_{20})_x(LiNbO_3)_{100-x}$ nanocomposite film deposition as a result of self-organization processes the amorphous layer of $LiNbO_3$ is formed on the surface of the Cr/Cu/Cr metal electrode, and the metal phase is displaced from NC/M interface into the bulk of the nanocomposite, which leads to the formation of metal nanogranules of a larger diameter than the equilibrium one, which is formed in the film bulk upon further deposition of the composite. At the same time, the physical nature of the processes that occur during such film deposition is not entirely clear.

3. Discussion

The model representation of the nanocomposites formation as a result of self-organization can be described as follows. Two types of atoms (A and B) come from the vapor phase to the substrate, they do not form solid solutions and chemical compounds with each other. As a result of surface diffusion the nuclei of phase A and phase B are formed. If the average diffusion distance is less than the radius of the nanoparticle, then atoms of A type

Values of surface energy of the phases included in the nanocomposites $(Co_{40}Fe_{40}B_{20})_x(LiNbO_3)_{100-x}$

Element	Surface energy of the solid phase, J/m^2
Cr	2.173 [23]
Fe	2.475 [23]
Co	2.550 [23]
Cu	1.356 [22]
$LiNbO_3$	0.039 [24]
	1.1 (012) and 0.65 (010) [25]

accumulate on the particle B surface and vice versa, thereby limiting the vertical growth of the granules. A homogeneous two-phase heterogeneous film is formed [18]. However, this representation does not describe the formation of a dielectric layer in the composite at the initial stages of $(Co_{40}Fe_{40}B_{20})_x(LiNbO_3)_{100-x}$ film growth.

Let us consider the possibility of forming a $LiNbO_3$ interlayer on the surface of a chromium metal film by implementing island and layer-by-layer growth mechanisms for different phases of the composite. By the first mechanism according to Volmer and Weber (VW), the film growth begins with the formation of discrete nuclei-islands on the surface of a solid state (substrate) [19]. As atoms arrive from the source (for example, an evaporator), the islands grow, combine, and form a labyrinth and then a solid coating. According to Frank and Van der Merwe (FM), film growth begins with the formation of two-dimensional nuclei and successive growth of monoatomic layers [20,21]. There are simple energy criteria for the implementation of one or another growth model. Thus, the VW mechanism is implemented when

$$E_1 < E_2 + E_{12} + E_\varepsilon(t),$$

where E_1 is the free energy of the substrate surface, E_2 — of the film, E_{12} — of the interface substrate−film, $E_\varepsilon(t)$ is the energy of elastic strain of the growing film.

On condition

$$E_1 \geq E_2 + E_{12} + E_\varepsilon(t)$$

layered film nucleation is more advantageous; i.e., according to FM mechanism. The Table shows the values of the surface energy of the phases that contained the nanocomposites $(Co_{40}Fe_{40}B_{20})_x(LiNbO_3)_{100-x}$.

The data given in the Table refer to solid materials. In the case of nanosized CoFe granules of limited thickness and an amorphous structure of the dielectric phase of $LiNbO_3$, the values of the surface energy can be slightly less [26].

Consider the relative energies E_{12} in the case of the interface Cr−CoFe, Cr−α−$LiNbO_3$ and α-$LiNbO_3$−CoFe. Cr and CoFe have BCC crystal lattice with parameters of 0.2885 and 0.29ṅm, respectively, which ensures the heteroepitaxial growth of nuclei of the metal phase on the substrate. This leads to a significant decrease in the interfacial energy E_{12} and a strong interfacial bonding. Cr does not have chemical compounds with $LiNbO_3$, however, it can form chemical bonds with lithium oxide ($LiCrO_2$, $LiCr_3O_8$ and Li_2CrO_4) and niobium oxide ($CrNbO_4$, $CrNb_{11}O_{29}$ and $CrNb_{49}O_{124}$). When such bonds are formed, the energy of the interface E_{12} can decrease. By determining the possibility of forming the nanocomposite, the phases included in its composition do not dissolve and do not have chemical compounds, so the interface α-$LiNbO_3$−CoFe has a weak interfacial bond.

Nevertheless, the presented data confirm our assumptions about the possibility of growing $LiNbO_3$ film by the FM mechanism, and metal granules by VW mechanism on the surface of the Cr film.

Consider the process of self-organization of $(Co_{40}Fe_{40}B_{20})_x(LiNbO_3)_{100-x}$ composites at the initial stage of film formation. At the initial moment of time, the atoms of the metallic phase form nuclei on the Cr surface. Chromium and CoFe nuclei have BCC lattice with good lattice cell size matching. Therefore, it can be assumed that the formation of a two-dimensional metal particle with heteroepitaxial structure relative to the Cr film will be energetically favorable. The film of the dielectric phase forms a monoatomic layer. This situation is shown in Fig. 2, *a*.

The ratio of $LiNbO_3$ compound molecules to CoFe in the sample $(Co_{40}Fe_{40}B_{20})_{15}(LiNbO_3)_{85}$ shown in Fig. 1 is ≈ 6.7. To form a homogeneous nanocomposite in the bulk of the film, the adatoms of $LiNbO_3$ molecule must have a small diffusion length on the substrate surface due to the amorphous state of $LiNbO_3$ structure and the oxide molecules accumulation on the surface of granule several nanometers in size. According to these reasons, the nuclei of the metallic phase are rapidly covered with the α-$LiNbO_3$ film. The next nuclei of the metallic phase will form on the surface of the α-$LiNbO_3$ film. An important assumption of this model is the presence of surface migration of CoFe islands. Numerous studies confirm that at the initial stage of crystalline films condensation on the substrate, the nuclei weakly bound to the deposited material can relatively quickly move over the surface [27–29]. This migration can be initiated by collisions with fast flow particles, temperature, electric and magnetic field gradients, etc. Note that in the case of the initial stage of composite formation the characteristic size of the potential surface relief is incommensurable with the size of CoFe particles, which is also a factor that allows nuclei to move over the surface. This situation is shown in Fig. 2, *b*.

The collision of metal particles migrating over the surface can lead to their coalescence. However, diffusion coalescence is limited by time and particles size. A shell from $LiNbO_3$ compound is formed on large particles. The contact of such particles does not lead to their merging. This film growth phase is shown in Fig. 2, *c*.

When metal granules with α-$LiNbO_3$ shells fill the entire surface of the substrate, the formation of the dielectric layer ends. A significant difference in the further process of nanocomposite formation is the formation of a potential

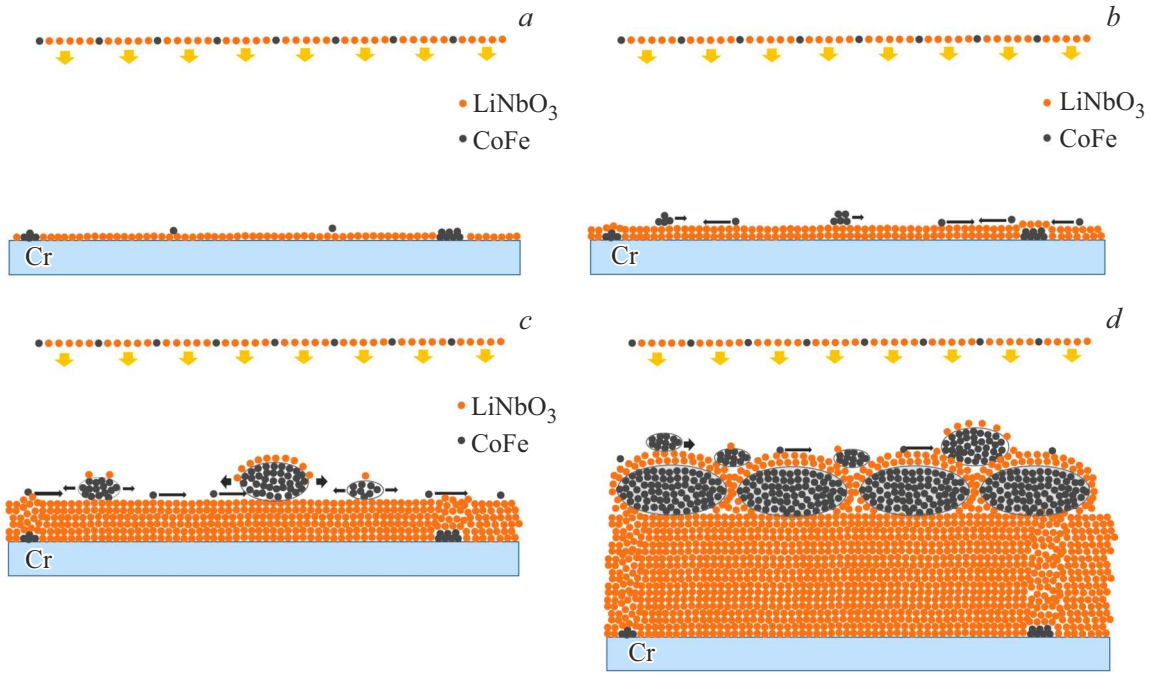

Figure 2. Model representations of $(Co_{40}Fe_{40}B_{20})_x(LiNbO_3)_{100-x}$ composites growth at the initial stage of film formation (a); at the initial stage of the dielectric layer formation of the film (b); at the stage of formation of enlarged granules of the metal phase of the film (c); formation of homogeneous nanosized heterogeneous structure (d).

relief on the surface, commensurate with the size of CoFe nanogranules. The concept of potential relief here includes not only the surface relief, but also the distribution of the magnetic field of CoFe ferromagnetic particles, the distribution of the magnetostatic fields of the dielectric layer, etc. This can significantly limit the diffusion mobility of CoFe metal alloy nuclei. In this case, the formation of a composite nanostructure proceeds according to the model described above. An uniform nanosized heterogeneous structure of $(Co_{40}Fe_{40}B_{20})_x(LiNbO_3)_{100-x}$ composite (Fig. 2, d) is formed.

The considered model concepts can be extended to numerous metal-dielectric nanocomposites formed on a metal film. Besides, it is obvious that the thickness of the dielectric layer will decrease with concentration increasing of the metal phase. This mechanism may not work in composites beyond the percolation threshold.

Conclusion

The above studies of the topological features of $(Co_{40}Fe_{40}B_{20})_{15}(LiNbO_3)_{85}$ nanocomposite films deposited on Cr/Cu/Cr metal electrode revealed the presence of a dielectric layer between the upper Cr layer and the NC film with a thickness of $d_{ox} \approx 15$ nm. A model representation of the formation of a film of $(Co_{40}Fe_{40}B_{20})_x(LiNbO_3)_{100-x}$ nanocomposites at the initial stage of growth was suggested. It is shown that the formation of the interlayer α-$LiNbO_3$ on the surface of chromium metal film is possible when the island and layer-by-layer growth mechanisms are realized for various NC phases. The model results can be extended to metal–dielectric nanocomposites formed on a metal film. The thickness of the dielectric layer will decrease with concentration increasing of the metal phase.

Acknowledgments

The authors are grateful to E.V. Kukueva for electron-microscopic studies and to V.V. Rylkov for help in discussing the results.

Funding

This study was supported financially by grant of Russian Foundation for Basic Research № 19-29-03022 mk.

Conflict of interest

The authors declare that they have no conflict of interest.

References

[1] A.N. Matsukatova, P.K. Kashkarov, A.V. Emelyanov, A.A. Minnekhanov, D.A. Sakharutov, A.Y. Vdovichenko, R.A. Kamyshinskii, V.A. Demin, V.V. Rylkov, P.A. Forsh, S.N. Chvalun. Tech. Phys. Lett., **46** (1), 73 (2020). DOI: 10.1134/S1063785020010277

[2] A.V. Arkhipov, G.V. Nenashev, A.N. Aleshin. FTT, **63** (4), 559 (2021) (in Russian) DOI: 10.21883/FTT.2021.04.50725.263

[3] W. Li, X. Liu, Y. Wang, Z. Dai, W. Wu, L. Cheng, Y. Zhang, Q. Liu, X. Xiao, C. Jiang. Appl. Phys. Lett., **108**, 153501 (2016). DOI: 10.1063/1.4945982
[4] M.N. Martyshov, A.V. Emelyanov, V.A. Demin, K.E. Nikiruy, A.A. Minnekhanov, S.N. Nikolaev, A.N. Taldenkov, A.V. Ovcharov, M.Yu. Presnyakov, A.V. Sitnikov, A.L. Vasiliev, P.A. Forsh, A.B. Granovsky, P.K. Kashkarov, M.V. Kovalchuk, V.V. Rylkov. Phys. Rev. Appl., **14**, 034016 (2020). DOI: 10.1103/physrevapplied.14.034016
[5] V.V. Rylkov, A.V. Emelyanov, S.N. Nikolaev, K.E. Nikiruy, A.V. Sitnikov, E.A. Fadeev, V.A. Demin, A.B. Granovsky. JETP, **131** (1), 160 (2020) DOI: 10.1134/S1063776120070109
[6] V.V. Rylkov, A.V. Sitnikov, S.N. Nikolaev, V.A. Demin, A.N. Taldenkov, M.Yu. Presnyakov, A.V. Emelyanov, A.L. Vasiliev, Yu.E. Kalinin, A.S. Bugaev, V.V. Tugushev, A.B. Granovsky. J. Magn. Magn. Mater., **459**, 197 (2018). DOI: 10.1016/j.jmmm.2017.11.022
[7] D. Ielmini. Semicond. Sci. Technol., **31**, 063002 (2016). DOI: 10.1088/0268-1242/31/6/063002
[8] W. Banerjee, Q. Liu, H. Hwang. J. Appl. Phys., **127**, 051101 (2020). DOI: 10.1063/1.5136264
[9] M. Zhuk, S. Zarubin, I. Karateev, Yu. Matveyev, E. Gornev, G. Krasnikov, D. Negrov, A. Zenkevich. Front. Neurosci., **14**, 94 (2020). DOI: 10.3389/fnins.2020.00094
[10] A. Mikhaylov, A. Belov, D. Korolev, I. Antonov, V. Kotomina, A. Kotina, E. Gryaznov, A. Sharapov, M. Koryazhkina, R. Kryukov, S. Zubkov, A. Sushkov, D. Pavlov, S. Tikhov, O. Morozov, D. Tetelbaum. Adv. Mater. Technol., **5** (1), 1900607 (2020). DOI: 10.1002/admt.201900607
[11] J. Valle, J.G. Ramírez, M.J. Rozenberg, I.K. Schuller. J. Appl. Phys., **124** (21), 211101 (2018). DOI: 10.1063/1.5047800
[12] Y. Li, Zh. Wang, R. Midya, Q. Xia, J.J. Yang. J. Phys. D: Appl. Phys., **51** (50), 503002 (2018). DOI: 10.1088/1361-6463/aade3f
[13] D.-H. Kwon, K.M. Kim, J.H. Jang, J.M. Jeon, M.H. Lee, G.H. Kim, X.-Sh. Li, G.-S. Park, B. Lee, S. Han, M. Kim, Ch.S. Hwang. Nat. Nanotechnol., **5**, 148 (2010). DOI: 10.1038/nnano.2009.456
[14] J.-Y. Chen, Ch.-W. Huang, Ch.-H. Chiu, Yu-T. Huang, W.-W. Wu. Adv. Mater., **27** (34), 5028 (2015). DOI: 10.1002/adma.201502758
[15] H. Jiang, L. Han, P. Lin, Zh. Wang, M.H. Jang, Q. Wu, M. Barnell, J.J. Yang, H.L. Xin, Q. Xia. Sci. Rep. **6**, 28525 (2016). DOI: 10.1038/srep28525
[16] S.A. Gridnev, Yu.E. Kalinin, A.V. Sitnikov, O.V. Stogney. *Nelineynye yavleniya v nano- i mikrogeterogennykh sistemakh* (BINOM, Laboratoriya znaniy, M., 2012) (in Russian)
[17] V.V. Rylkov, V.A. Demin, A.V. Emelyanov, A.V. Sitnikov, Yu.E. Kalinin, V.V. Tugushev, A.B. Granovsky. *Novel Magnetic Nanostructures: Unique Properties and Applications*, ed. by N. Domracheva, M. Caporali, E. Rentschler (Elsevier, 2018), p. 427.
[18] V.M. Ievlev. *Tonkie plenki neorganicheskikh materialov: mekhanizm rosta i struktura* (Izdat.-polygraf. tsentr Voronezh. gos. un-ta, Voronezh, 2008) (in Russian)
[19] M. Volmer, A. Weber. Z. Phys. Chem., **119** (3/4), 277 (1926). DOI: 10.1515/zpch-1926- 11927
[20] F.C. Frank, J.H. Van der Merve. Proc. Roy. Soc. A, **198**, 205 (1949). DOI: 10.1098/rspa.1949.0095
[21] F.C. Frank, J.H. Van der Merve. Proc. Roy. Soc. A, **200**, 125 (1949). DOI: 10.1098/rspa.1949.0163
[22] V.M. Yurov, V.Ch. Laurinas, S.A. Guchenko, O.N. Zavatskaya. Sovremennye naukoemkie tekhnologii, **3**, 36 (2012) (in Russian)
[23] S.Yu. Lazarev. Metalloobrabotka, **2** (14), 38 (2003) (in Russian)
[24] B. Baker, N. Herbots, Sh.D. Whaley, M. Sahal, J. Kintz, A. Yano, S. Narayan, A.L. Brimhall, W.-L. Lee, Y. Akabane, R.J. Culbertson. J. Vac. Sci. Technol. A, **37**, 041101 (2019). DOI: 10.1116/1.5095157
[25] Y. Hirsh, S. Gorfman, D. Sherman. Acta Mater., **193**, 338 (2020). DOI: j.actamat.2020.03.046
[26] V.M. Samsonov, A.A. Chernyshova, N.Yu. Sdobnyakov. Izv. RAN. Ser. fiz., **80** (6), 768 (2016) (in Russian). DOI: 10.7868/S0367676516060296
[27] R. Kern, G.L. Lay, J.J. Metois. Curr. Top. Mater. Sci., **3**, 131 (1979).
[28] V.P. Rubetz, S.A. Kukushkin. Thin Solid Films, **221**, 267 (1992). DOI: 10.1016/0040-6090(92)90825-v
[29] R. Kern, A. Masson, J.J. Métois, Surf. Sci., **27**, 483 (1971). DOI: 10.1016/0039-6028(71)90183-X